

SOLID-STATE MICROSTRUCTURE EVOLUTION IN STEELS

Victor D. Fachinotti, Alberto Cardona and Andrés A. Anca

Centro Internacional de Métodos Computacionales en Ingeniería (CIMEC)
Universidad Nacional del Litoral (UNL) /
Consejo Nacional de Investigaciones Científicas y Técnicas (CONICET)
Ruta 168, Paraje El Pozo, 3000, Santa Fe, Argentina
e-mails: vfachino@intec.unl.edu.ar, acardona@intec.unl.edu.ar, aanca@intec.unl.edu.ar

Key Words: IT, CCT, continuous cooling, microstructure evolution, eutectoid steels, pearlitic transformation, martensitic transformation.

Abstract. *This paper deals with the simulation of microstructure evolution in steels, specifically eutectoid steels, where competitive diffusive (pearlitic) and diffusionless (martensitic) transformations may take place.*

Diffusion-controlled transformations are modelled by using the classical Johnson-Mehl-Avrami-Kolmogorov law for isothermal transformations, while the martensitic transformation is assumed to obey either the Koistinen-Marburger or the Yu laws.

The non-isothermal evolution of diffusive transformations is derived from the isothermal transformation kinetics either by invoking the additivity rule, or by integrating the rate form of the Johnson-Mehl-Avrami-Kolmogorov law in time. The ability of both techniques to build continuous cooling transformation (CCT) diagrams from isothermal transformation (IT) diagrams is evaluated.

Microstructure evolution is coupled with the thermal analysis, performed using the finite element method.

A finite element analysis of a quench problem is finally carried out to evaluate the performance of the model.

1 INTRODUCTION

This paper aims to modelling the evolution of the microstructure in a material undergoing heat treatment. This stage of the study is focused on monophasic transformations on eutectoid steels during continuous cooling processes.

An eutectoid carbon steel, initially austenitic, transforms either to pearlite or martensite depending on the cooling rate. The austenite→pearlite transition is driven by the diffusion of carbon atoms, and hence it is time-dependent. On the other hand, austenite→martensite transformation is diffusionless.

The transformation kinetics is described by means of isothermal-transformation (IT) diagrams (also known as TTT-diagrams), usually obtained by dilatometry. Diagrams for general cooling and heating conditions are derived from IT-diagrams making appeal to the Scheil's additivity rule: a general thermal history is described as a series of isothermal steps. Strictly speaking, the additivity rule holds only for isokinetic reactions, i.e., reactions where the nucleation rate is proportional to the growth rate. Nevertheless, in practice it has been applied satisfactorily to more general transformations.¹⁻³

Some researchers^{4,5} criticized the broad use of the additivity rule, and proposed more sophisticated models. These works are based on the integration of the rate form of the Johnson-Mehl-Avrami-Kolmogorov (JMAK) law, which defines diffusion-controlled transformations under isothermal conditions.

In this paper, the JMAK law itself (i.e., not its rate form) is used together with the additivity rule in order to model non-isothermal transformations. We compare this model with the JMAK-rate model proposed by Lusk and Jou⁴ for computing diffusion-controlled transformation under continuous cooling. We show that the method based on the additivity rule is simpler and provides better accuracy than the rate-based one. Last, but not least, the model based on the additivity rule is cheaper to compute.

Regarding the diffusionless martensitic transformation, we apply the widely used Koistinen-Marburger law. However, as it will be demonstrated, this law is not able to model complete transformations. So, an alternative law proposed by Yu,¹⁹ capable of modelling such transformations, is also tested.

Finally, the present model will be applied for simulating the Jominy end-quench test, comparing our results with available experimental and numerical data.

2 MODELLING OF DIFFUSION-CONTROLLED TRANSFORMATIONS

The evolution of the transformed constituent is described by using the Johnson-Mehl-Avrami-Kolmogorov (JMAK) law, which is the most commonly used model for describing diffusive transformations kinetics. This law defines the volume fraction p of the product constituent at time t for an isothermal transformation at temperature T as

$$p = P [1 - \exp(-bt^a)], \quad (1)$$

where a , b and P are parameters that depend on the temperature T held all along the transformation.

The coefficients $a = a(T)$ and $b = b(T)$ are determined by knowing two points in the IT-diagram of the material being modelled for the given temperature T . The parameter $P = P(T)$ is the maximum fraction of product constituent that can be formed along the isothermal transformation at temperature T . If $P = 1$ the transformation is said to be complete. In general, P has to be determined experimentally by measuring the fraction of each constituent present at the end of each isothermal transformation. For proeutectoid constituents (ferrite, cementite), the value of P can be deduced from the equilibrium diagram using Hultgren extrapolation.^{1,6}

In order to track the evolution of the microstructure during a non-isothermal diffusion-driven transformation, two alternatives will be explored: the use of the additivity rule, and the integration of the rate form of the JMAK equation (1) in time, as detailed below.

2.1 The additivity-rule (AR) model

According to the additivity rule, we can represent any non-isothermal transformation as a series of steps $i = 1, 2, \dots$ where the temperature is maintained at a constant value T_i during a period Δt_i .

Let p_i be the fraction transformed at the end of the isothermal step i , carried out at temperature T_i , which is taken as the initial fraction for the next isothermal step $i + 1$ developed at temperature T_{i+1} . The fraction at the end of this step is determined by

$$p_{i+1} = P_{i+1} (1 - \exp(-b_{i+1}(t_i^* + \Delta t_{i+1})^{a_{i+1}})), \quad (2)$$

where $P_{i+1} = P(T_{i+1})$, $a_{i+1} = a(T_{i+1})$, $b_{i+1} = b(T_{i+1})$, Δt_{i+1} is the duration of the step $i + 1$, and t_i^* is a fictitious time defined to be the time needed to obtain p_i during the isothermal transformation at temperature T_{i+1} , i.e.

$$t_i^* = \left(\frac{1}{b_{i+1}} \ln \frac{P_{i+1}}{P_{i+1} - p_n} \right)^{1/a_{i+1}}. \quad (3)$$

2.2 The JMAK-rate model

Mathematically, it can be shown^{4,5} that the transformation described by equation (1) is isokinetic only if a does not depend on temperature. If it is not the case, the additivity rule is no longer valid in a strict mathematical sense. Therefore, the evolution of the transformed phase during non-isothermal processes should not be modelled as a series of isothermal steps but computed by integrating the rate form of the JMAK equation, written as the autonomous differential equation

$$\dot{p} = b^{1/a} a (P - p) \left(\ln \frac{P}{P - p} \right)^{1-1/a} \quad \forall t > 0, \quad (4)$$

$$p(0) = p_0, \quad (5)$$

where the superimposed dot indicates time derivative.

Regarding the initial condition, p_0 should be null but it is often assigned a small value in order to facilitate the numerical integration of equation (4), particularly when explicit methods are used.

In order to integrate equation (4), the following single-step algorithm will be used:

$$\frac{p_{i+1} - p_i}{\Delta t_{i+1}} = b_{i+\theta}^{1/a_{i+\theta}} a_{i+\theta} (P_{i+\theta} - p_{i+\theta}) \left(\ln \frac{P_{i+\theta}}{P_{i+\theta} - p_{i+\theta}} \right)^{1-1/a_{i+\theta}}, \quad (6)$$

where, for any variable λ ,

$$\lambda_{i+\theta} = \lambda_i + \theta(\lambda_{i+1} - \lambda_i) \quad (7)$$

with $0 \leq \theta \leq 1$. Particularly, $\theta = 0$ gives the explicit, conditionally stable, first-order accurate forward-Euler (fE) method; $\theta = 1$ gives the implicit, unconditionally stable, first-order accurate backward-Euler (bE) method, and $\theta = 0.5$ gives the implicit, unconditionally stable, second-order accurate Crank-Nicolson (fE) method. For the implicit methods, equation (6) is nonlinear and has to be solved numerically using iterative methods.

2.3 Generating CCT-diagrams from a IT-diagram

Let us consider the pearlite portion of the IT-diagram of a SAE 6150 steel, as defined by Lusk and Jou,⁴ with:

$$a = 3.76 + 0.0235(600 - T), \quad (8)$$

$$b = 4.3099 \times 10^{-10} \exp \left(-4.2355 \left(\exp \left(4.9374 \times 10^{-5} (602.55 - T)^2 \right) \right)^2 \right), \quad (9)$$

where T is given in degrees Celsius. The C-curves corresponding to 1% and 99% of transformed phase are plotted with solid lines in Figure 1.

Lusk and Jou's CCT-diagram was obtained for an unspecified exponential cooling history. Here, in an attempt to approach Lusk and Jou's conditions, the following exponential cooling law is imposed

$$T = T_s - \frac{\exp(ct) - 1}{\exp(ct_f) - 1} (T_s - T_f), \quad (10)$$

where T is given in degrees Celsius, t in seconds, $c = 5. \times 10^{-4}$, $T_s = 660^\circ\text{C}$, $T_f = 430^\circ\text{C}$, and t_f is the time spent to cool from T_s to T_f , varying between $10^{2.2}$ to 10^4 sec. Further, in order to compare with Lusk and Jou's results, the transformation is assumed to be complete (i.e., $P = 1$) in the whole range of temperatures considered.

The time step Δt , defining either the duration of each isothermal step when the additivity rule is applied or the time step used for integrating equation (4), is set to $t_f/4000$.

Figure 1 shows the CCT-diagram computed on the basis of the given IT-diagram using both the model based on the additivity rule and the JMAK-rate model.

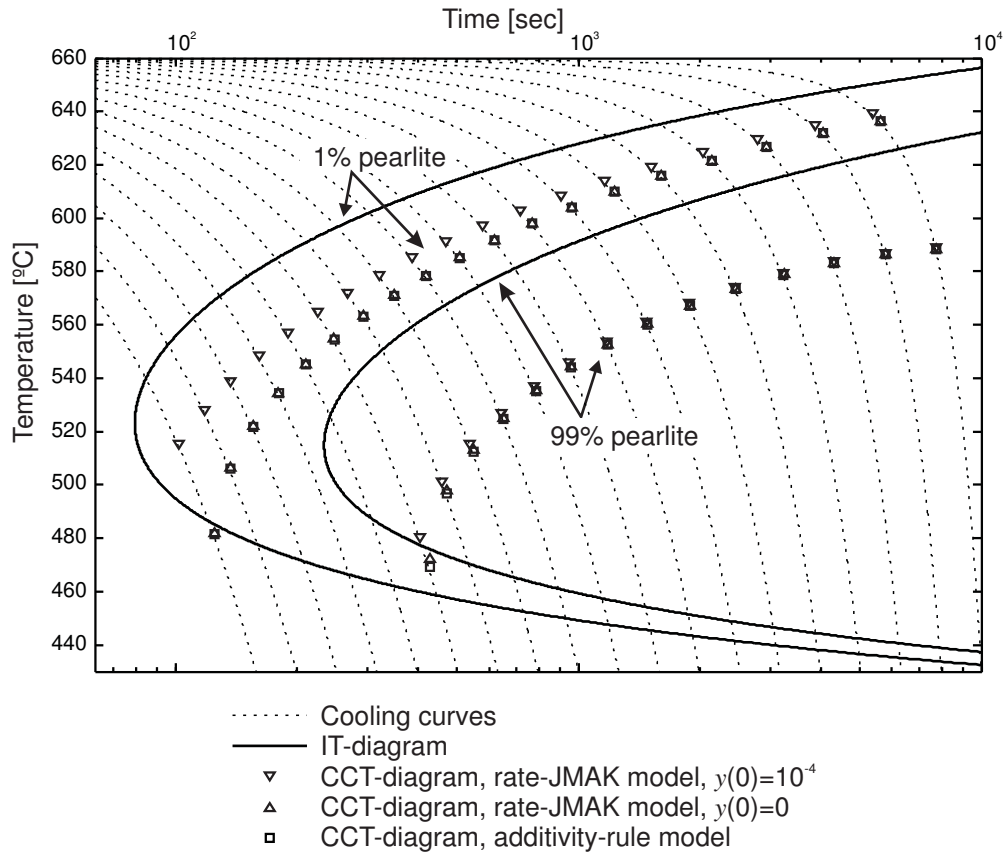


Figure 1: IT-diagram and derived CCT-diagrams

When equation (4) is solved with $p = 10^{-4}$ as initial condition (the value 10^{-4} is recommended in several articles by Lusk and coworkers⁷⁻¹⁰), a certain difference with the results obtained by using the AR model is observed. The difference is similar to that observed in⁴ which had motivated these authors to criticize the applicability of the additivity rule for transformations kinetics where a depends on temperature. However, taking strictly $p(0) = 0$, the solution of equation (4) is in excellent agreement with that obtained by the additivity rule.

Now, in order to test accuracy with respect to the time step size, the AR model and the rate-JMAK model integrated with fE, bE and CN methods were applied to predict the pearlite fraction at the end of the exponential cooling history given by equation (10) with $t_f = 5$ min, that is

$$T = 660. - 1421.207 (\exp(0.0005t) - 1), \tag{11}$$

where T is given in degrees Celsius and t in seconds.

The computed pearlite fractions are plotted on the left of Figure 2.

In order to evaluate the evolution of the error as the time step increases, considering that an exact analytical solution does not exist, the exact value p_{exact} is approximated by the average

of the different numerical solutions for an extremely fine time step (0.01 sec), $p_{exact} \approx p_{ave} = 0.36360496$.

As shown on the right of Figure 2, compared to fE- and bE-rate-JMAK models, the AR model has the same convergence rate but its error is two-orders-of-magnitude smaller than the former ones. The CN-rate-JMAK model converges faster than fE- and bE-rate-JMAK models, but its accuracy remains poorer than that of the AR model for typical time step sizes (0.1 to 1 sec), and as poor as fE- and bE-rate-JMAK models for larger time steps.

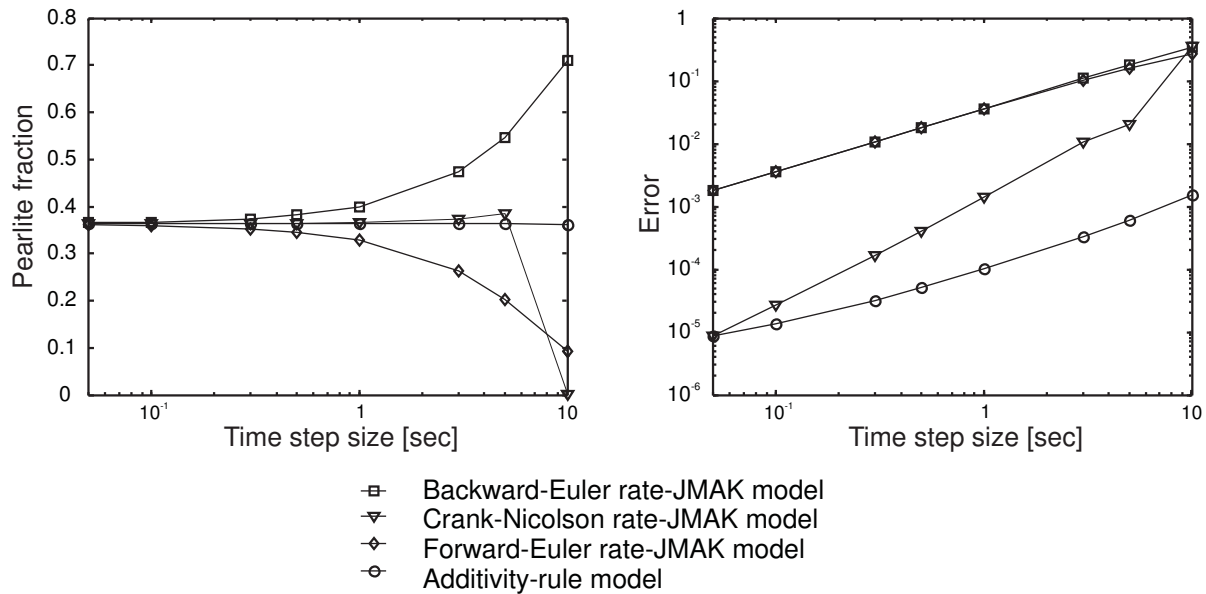


Figure 2: Pearlite fraction after 5 min for the cooling history given by equation (11), as a function of the time step used for tracking the fraction evolution.

Regarding computational cost, the fE-rate-JMAK and AR models are the cheaper ones, since the function for updating p is explicit. On the other hand, using bE- and CN-rate-JMAK models, the evolution of p is governed by a nonlinear equation to be solved numerically by an iterative process. Additionally, as demonstrated by the influence of the initial value p_0 , at the beginning of the transformation very small variations of p correspond to large variations of t , and in such case equation (6) must be solved with a very strict convergence criterium (we adopt here 10^{-12} for the variation of p), which increases the computational cost.

Therefore, regarding accuracy and computational cost, we conclude that the AR model results the best scheme for numerical modelling of non-isothermal transformations, even if the transformation is not isokinetic.

3 MODELLING OF MARTENSITIC TRANSFORMATION

Contrary to diffusion-controlled transformations, the martensitic transformation is diffusionless and takes place only in non-isothermal processes. The formation of martensite during cooling

begins at temperature M_s , and its volume fraction is usually computed using the Koistinen-Marburger law:

$$m = \bar{\gamma} (1 - \exp(-k(M_s - T))), \quad T < M_s, \quad (12)$$

where $\bar{\gamma}$ is the residual volume fraction of austenite at M_s , and k characterizes the evolution of the transformation with temperature, usually taken equal to 0.011 for steels. In this work, $\bar{\gamma}$ represents the austenite not already transformed into pearlite once the temperature M_s is reached during the cooling process.

We choose to track the evolution of the martensite fraction by applying equation (12) straightforwardly, as done by Murthy et al,¹¹ Boyadjiev et al,¹² Bokota and Iskierka,² Alberg and Berglund,¹³ Prieto et al,¹⁴ Costa et al,¹⁵ Casotto et al,¹⁶ and contrary to the proposal of Bammann et al,⁷ Holmberg,^{17,17} Prantil et al¹⁸ who solve the rate form of equation (12).

Alternatively, we apply the parabolic law proposed by Yu,¹⁹ which defines the martensite volume fraction as:

$$m = \bar{\gamma} \left(1 - \left(\frac{T - M_f}{M_s - M_f} \right)^2 \right), \quad T < M_s, \quad (13)$$

being M_f the transformation finish temperature.

4 THE HEAT EQUATION

Temperature distribution in the domain of interest Ω is governed by the heat conduction equation

$$\rho \dot{\mathcal{H}} - \nabla \cdot (\kappa \nabla T) = 0, \quad \forall \mathbf{x} \in \Omega, \forall t > 0, \quad (14)$$

subject to the initial condition

$$T = T_0(\mathbf{x}), \quad \forall \mathbf{x} \in \Omega, t = 0, \quad (15)$$

and the following boundary conditions on the closure $\partial\Omega$:

$$T = \bar{T}(\mathbf{x}, t), \quad \forall \mathbf{x} \in \partial\Omega_T, \forall t > 0, \quad (16)$$

$$\kappa \nabla T \cdot \mathbf{n} = \bar{q}(\mathbf{x}, t), \quad \forall \mathbf{x} \in \partial\Omega_q, \forall t > 0, \quad (17)$$

$$\kappa \nabla T \cdot \mathbf{n} = h(T)(T_{env} - T), \quad \forall \mathbf{x} \in \partial\Omega_{c/r}, \forall t > 0, \quad (18)$$

In the above equations, \mathcal{H} is the enthalpy per unit mass, ρ is the material density, and κ the thermal conductivity; regarding boundary conditions, $\partial\Omega_T$, $\partial\Omega_q$ and $\partial\Omega_{c/r}$ denote non-overlapped portions of $\partial\Omega$, \mathbf{n} the unit normal vector pointing outwards $\partial\Omega$, \bar{T} and \bar{q} prescribed values of the temperature and the heat flux, respectively, h is the heat convection or radiation coefficient, and T_{env} the temperature of the external environment.

Bulk properties, like ρ , \mathcal{H} and κ , are defined by the mixture law

$$\lambda = m\lambda_m + p\lambda_p + \gamma\lambda_\gamma, \quad (19)$$

where λ_i is the property restricted to constituent i ($i = m, p, \gamma$), and $\gamma = 1 - m - p$ is the volume fraction of austenite. Each property λ_i may be thermodependent.

4.1 Discretization of the thermal problem

First, the equation (14) is integrated in time using the Euler-backward implicit time-stepping scheme. The temperature T at time $t = t_0 + \Delta t$ is determined by the equation:

$$\rho \frac{\mathcal{H} - \mathcal{H}^0}{\Delta t} - \nabla \cdot (\kappa \nabla T) = 0, \quad (20)$$

where the superindex 0 denotes quantities referred to the previous time instant t_0 , assumed to be known.

Finally, the fully-discrete version of the heat equation is obtained by applying the finite element method (FEM) for spatial discretization. The unknown temperature field T is approximated as follows:

$$T(\mathbf{x}, t) = N_i(\mathbf{x})T_i(t), \quad \forall \mathbf{x} \in \Omega, \forall t > 0, \quad (21)$$

where N_i is the shape function associated to node i and T_i the unknown temperature at this node.

Introducing this approximation into the weak form of equation (20), with the shape functions playing the role of the weighting functions (i.e., Galerkin formulation), we obtain

$$\frac{H_i - H_i^0}{\Delta t} + K_{ij}T_j - F_i = 0, \quad (22)$$

where H_i is the enthalpy vector, K_{ij} is the conductivity (or stiffness) matrix, and F_i is the external heat flux vector, each one defined as

$$H_i = \int_{\Omega} \rho \mathcal{H} N_i dV, \quad (23)$$

$$K_{ij} = \int_{\Omega} \kappa \nabla N_i \cdot \nabla N_j dV, \quad (24)$$

$$F_i = \int_{\partial\Omega_q} \bar{q} N_i dS + \int_{\partial\Omega_{c/r}} h(T_{env} - N_j T_j) N_i dS. \quad (25)$$

The above integrals are computed numerically. At each integration point, the constituents fractions are computed using the strategy developed in the previous section.

The non-linear system of algebraic equations (22) is solved using the Newton-Raphson method.

Remark: The time step used for integrating the heat equation, say Δt_{HE} , does not need to be equal to that defined as the duration of the isothermal steps when the additivity rule is used, say Δt_{AR} . In fact, while reducing Δt_{AR} improves the accuracy for tracking microstructure evolution, the decrease of Δt_{HE} may cause numerical instabilities as it is the case in presence of thermal shocks,²⁰ and hence in the modelling of rapid cooling processes.

Taking these considerations into account, we decide to uncouple the choice of Δt_{HE} and Δt_{AR} , being always $\Delta t_{HE} \geq \Delta t_{AR}$.

5 APPLICATION

Let us consider the Jominy end-quench test, as treated by Hömberg.¹⁷ The material is an eutectoid carbon steel C1080, whose IT-diagram is observed in Figure 3. This diagram is digitalized by taking a series of points (t, T) on two C-curves. Intermediate values are obtained by piecewise-cubic Hermite interpolation based on the gathered points.

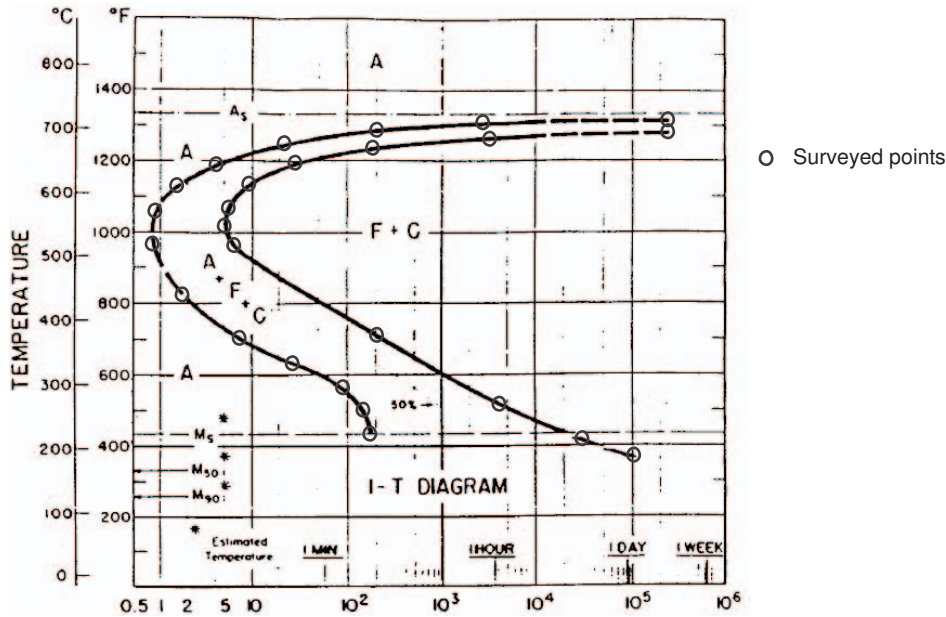


Figure 3: IT-diagram for C1080 steel.

Then, taking one point on each curve for a given temperature T , the parameters $a(T)$ and $b(T)$ of the JMAK law are computed. The so-determined values of a and b are plotted in Figure 4.

Average values are adopted for the mass density ($\rho = 7200.\text{kg}/\text{m}^3$), the thermal conductivity ($\kappa = 34.\text{W}/(\text{m}^\circ\text{C})$) as well as for the specific heat ($c_p = 680.\text{J}/(\text{kg}^\circ\text{C})$) used to define the sensible part of the enthalpy of each constituent. The total enthalpy \mathcal{H} is defined as

$$\mathcal{H} = c_p T - L_p p - L_m m, \quad (26)$$

where $L_p = 77000.\text{J}/\text{kg}$ and $L_m = 84000.\text{J}/\text{kg}$ are the latent heats released during pearlitic and martensitic transformations, respectively.

For martensitic transformation, we assume $M_s = 224^\circ\text{C}$ and $M_f = 100^\circ\text{C}$, values that have been estimated from the IT-diagram in Figure 3.

The domain of interest consists of a cylindrical specimen, with radius $R = 1.25$ cm and length $L = 6.25$ cm, which is initially fully austenitic at homogeneous temperature $T^0 = 720^\circ\text{C}$, and suddenly cooled by applying a water jet to the lower end, according to the convec-

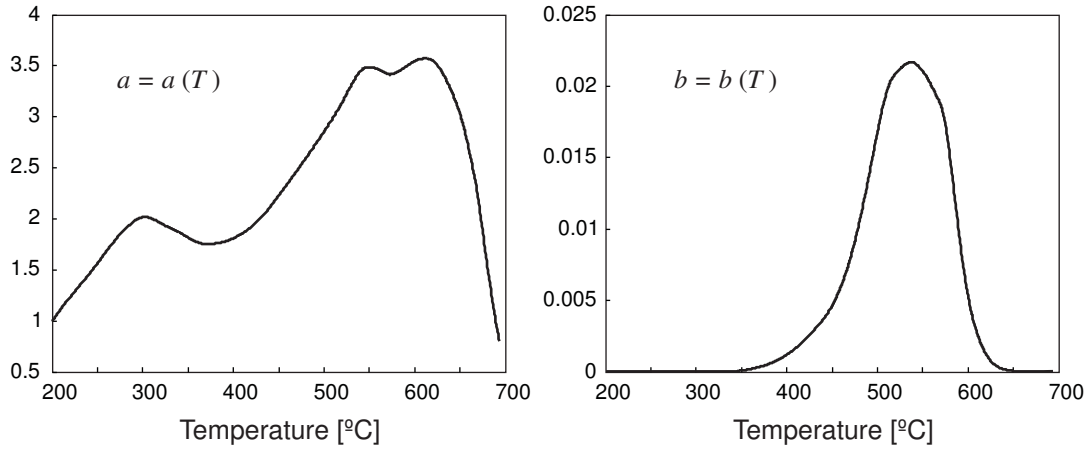


Figure 4: Parameters for the Johnson-Mehl-Avrami-Kolmogorov law computed from the IT-diagram for C1080 steel.

tion heat exchange law:

$$q_{wj} = h_{wj}(T)(T_{wj} - T), \quad (27)$$

with $T_{wj} = 25.^\circ\text{C}$, and

$$h_{wj}(T) = -1670. + 108.T - 0.0977.T^2 \quad (28)$$

given in $\text{W}/(^\circ\text{C m}^2)$ for T in $^\circ\text{C}$.¹⁷

Additionally, the specimen exchanges heat with the environment through its lateral surface. This heat flux is mainly radiative and is defined as²¹

$$q_{ls} = \varepsilon\sigma(T_{env}^4 - T^4), \quad (29)$$

where $\varepsilon = 0.8$ is the emissivity of the surface, σ is the Stefan-Boltzmann constant, and $T_{env} = 25.^\circ\text{C}$ is the environment temperature. We make this boundary conditions fit equation (18) by defining the non-linear radiative heat transfer coefficient

$$h_{ls}(T) = \varepsilon\sigma(T_{env}^2 + T^2)(T_{env} + T). \quad (30)$$

The upper end is supposed to be adiabatic.

Linear tetrahedra finite elements are used for the spatial discretization of the cylinder, as shown in Figure 5. Considering that the specimen as well as the boundary conditions are symmetric with respect to the axis of the specimen, just the cylinder generated by a small sector of the cross section is modelled. Even if an axisymmetric model is best suited for this particular problem in terms of computational cost, a 3D model is used keeping in mind future industrial applications.

The heat equation is integrated in time using a time step $\Delta t_{HE} = 0.5$ sec, while the duration of each isothermal step is $\Delta t_{AR} = 0.1$ sec.

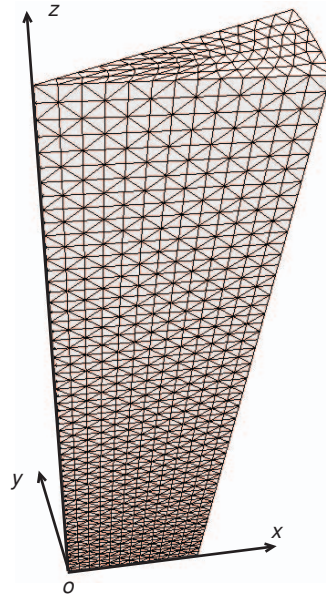


Figure 5: Linear tetrahedral finite element mesh of a longitudinal sector the specimen.

Figure 6 shows the distribution of the different constituents along the axis of the specimen, as computed using the different models. First, let us consider the case of martensitic transformation defined by widely used KM equation (12). At the quenched end ($z = 0$), the material is mainly martensitic ($\approx 89\%$), with a small fraction of retained austenite ($\approx 11\%$). From this end to a section located at $z \approx 7$. mm, the material present the three constituents: martensite, austenite and pearlite. The remaining material is predicted to have a fully pearlitic microstructure. Compared to experimental results²² as well as to previous numerical results,¹⁷ the martensite fraction is underestimated at the quenched end. However, the so-estimated width of the martensitic region is closer to the experimental result²² than that of Hömberg.¹⁷

The underestimation of the martensite fraction is associated to the use of the KM formula. In fact, equation (12) evaluated at the lowest temperature attainable during the cooling process $T_{min} = T_{wj} = T_{env} = 25^\circ\text{C}$ gives $m(T_{min}) \leq 88.80\% = m_{max}$, that is the maximum martensite fraction attainable under the present conditions.

The Yu law¹⁹ for martensite evolution enables the modelling of the complete austenite decomposition into martensite by introducing the temperature M_f such that $m(M_f)/\bar{\gamma} = 1$. The current model using Yu law for martensitic transformation gives the better results in terms of agreement with the experimental measures.²² In this case, no austenite is retained at the end of the process. Note that the pearlite fraction is practically identical to that computed using the KM law for martensite evolution.

6 CONCLUSIONS

The additivity rule has been found to be the best method to track the evolution of the microstructure evolution during cooling processes. The AR model was not only the most accurate scheme

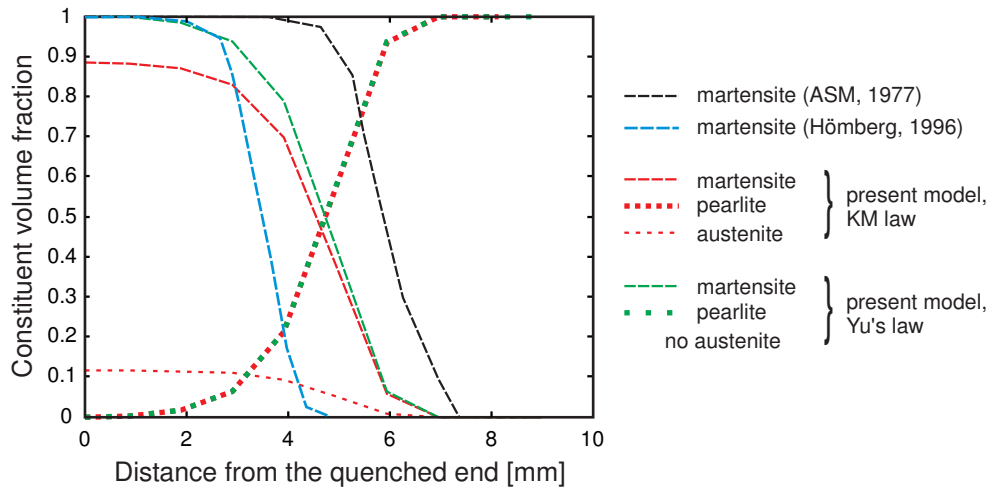


Figure 6: Volume fraction of the different constituent along the axis of the specimen.

for typical time step sizes but also one of the cheaper. Further, the AR model has proved to work not only for isokinetic transformations.

The evolution of the microstructure has been coupled with the solution of the heat equation in the three-dimensional space, giving a complete tool for the thermal analysis of cooling processes.

The time steps for integrating the heat equation and the microstructure evolution can be chosen independently.

The model has been applied to simulating the Jominy end-quench test, showing qualitatively satisfactory results compared to experiments. Differences with the experiments are mainly due to the use of the Koistinen-Marburger law for describing martensitic transformation. With this law, the modelling of a complete transformation is unfeasible for the range of temperatures of interest. This has been overcome by using the Yu law, which takes into account the temperature for which the transformation finishes.

The extension of the present model to general heat treatment processes will also be studied in future works.

REFERENCES

- [1] S. Denis, D. Farias, and A. Simon. Mathematical model coupling phase transformations and temperature evolutions in steels. *ISIJ International*, 32(3):316–325, 1992.
- [2] A. Bokota and S. Iskierka. Numerical analysis of phase transformations and residual stresses in steel cone-shaped elements hardened by induction and flame methods. *Int. J. Mech. Sci.*, 40(6):617–629, 1998.
- [3] D. Hömborg. Irreversible phase transitions in steel. *Mathematical Methods in Applied Sciences*, 20(1):59–77, 1997.
- [4] M. Lusk and H.-J. Jou. On the rule of additivity in phase transformations kinetics. *Metallurgical and Materials Transactions A*, 28:287–291, 1997.

- [5] T. Réti and I. Felde. A non-linear extension of the additivity rule. *Computational Materials Science*, 15:466–482, 1999.
- [6] F. Fernandes, S. Denis, and A. Simon. Prédiction de l'évolution thermique et structurale des aciers au cours de leur refroidissement continu. *Mémoires et Etudes Scientifiques Revue de Métallurgie*, 83:355–366, Juillet-Août 1986.
- [7] D. Bammann, V. Prantil, A. Kumar, T. Lowe, H.-J. Jou, M. Lusk, G. Krauss, B. Dowl- ing, B. Elliott, Jr, G. Ludtka, D. Shick, and D. Nikkel. Development of a carburizing and quenching simulation tool: A material model for carburizing steels undergoing phase transformations. In G. Totten, M. Howes, S. Sjöstrom, and K. Funatani, editors, *Proceed- ings of the Second International Conference on Quenching and the Control of Distortion*, pages 367–375, Cleveland, Ohio, November 1996.
- [8] M. T. Lusk and Y.-K. Lee. A global material model for simulating the transformation kinetics of low alloy steels. In J. Lendvai and T. Reti, editors, *Proceedings of the 7th. In- ternational Seminar of IFHT on Heat Treatment and Surface Engineering of Light Alloys*, pages 273–282, Budapest, September 1999. Hungarian Scientific Society of Mechanical Engineering (GTE).
- [9] M. T. Lusk, R. Jaramillo, A. Roche, C. Mgbokwere, and S. Deshpande. Microstructural evolution in sprayformed steel: Phase transitions, inelasticity, residual stress and distor- tion. In R. Srinivasan, S. Semiatin, A. Beaudoin, S. Fox, and Z. Jin, editors, *Microstruc- tural Modeling and Prediction During Thermomechanical Processing*, pages 75–84, War- rendale, PA, 2001. The Minerals, Metals and Materials Society.
- [10] M. T. Lusk, W. Wang, X. Sun, and Y.-K. Lee. On the role of kinematics in constructing predictive models of austenite decomposition. In E. B. Damm and M. J. Merwin, edi- tors, *Austenite Formation and Decomposition*, pages 311–332, Warrendale, PA, 2003. The Minerals, Metals and Materials Society.
- [11] Y. V. L. N. Murthy, G. Venkata Rao, and P. Krishna Iyer. Numerical simulation of welding and quenching processes using transient thermal and thermo-elasto-plastic formulations. *Computers & Structures*, 60(1):131–154, 1996.
- [12] I. I. Boyadjiev, P. F. Thomson, and Y. C. Lam. Computation of the diffusional transforma- tion of continuously cooled austenite for predicting the coefficient of thermal expansion in the numerical analysis of thermal stress. *ISIJ International*, 36(11):1413–1419, 1996.
- [13] H. Alberg and D. Berglund. Comparison of plastic, viscoplastic, and creep models when modelling welding and stress relief heat treatment. *Comput. Methods Appl. Mech. Engrg.*, 192:5189–5208, 2003.
- [14] E. Prieto Silva, P. M. Calas Lopes Pacheco, and M. Amorim Savi. On the thermo- mechanical coupling in austenite-martensite phase transformation related to the quenching process. *Int. J. Solids Structures*, 41:1139–1155, 2004.
- [15] L. Costa, R. Vilar, T. Reti, and A. M. Deus. Rapid tooling by laser powder deposition: Process simulation using finite element analysis. *Acta Materialia*, 53(14):3987–3999, 2005.
- [16] S. Casotto, F. Pascon, A. M. Habraken, and S. Bruschi. Thermo-mechanical-metallurgical

- model to predict geometrical distortions of rings during cooling phase after ring rolling operations. *Int. J. Machine Tools & Manufacture*, 45(6):657–664, 2005.
- [17] D. Hömberg. A numerical simulation of the Jominy end-quench test. *Acta Materialia*, 44(11):4375–4385, 1996.
- [18] V. C. Prantil, M. L. Callabresi, J. F. Lathrop, G. S. Ramaswamy, and M. T. Lusk. Simulating distortion and residual stresses in carburized thin strips. *Trans. ASME J. Engineering Materials and Technology*, 125:116–124, April 2003.
- [19] H. J. Yu. *Berechnung von Abkühlungs-, Umwandlungs-, Schweiss-, sowie Verformungsseignenspannungen mit Hilfe der Methode der finiten Elemente*. PhD thesis, Universität Karlsruhe, Germany, 1977.
- [20] V. D. Fachinotti and M. Bellet. Linear tetrahedral finite elements for thermal shock problems. Accepted, *Int. J. Numerical Methods in Heat and Fluid Flow*, 2005.
- [21] P. Le Masson, T. Loulou, E. Artioukhine, P. Rogeon, D. Carron, and J.-J. Quemener. A numerical study for the estimation of a convection heat transfer coefficient during a metallurgical “Jominy end-quench” test. *Int. J. Thermal Sciences*, 41:517527, 2002.
- [22] American Society for Metals. *Atlas of isothermal transformation and cooling transformation diagrams*, 1977.
- [23] H. Çetinel, M. Toparlı, and L. Özsoyeller. A finite element based prediction of the microstructural evolution of steels subjected to the tempcore process. *Mechanics of Materials*, 32:339–347, 2000.